Bangladesh J. Bot. **52**(2): 575-584, 2023 (June) Special DOI: https://doi.org/10.3329/bjb.v52i20.68227

HYPERSPECTRAL MULTIVARIATE LINEAR PREDICTION MODEL OF TOBACCO (*NICOTIANA TABACUM* L.) LEAF NITROGEN CONTENT

TING GUO[1*], WEN LI[1], LIANGYONG LI[2] AND XIMING ZOU[3]

Hunan Tobacco Company Chenzhou Company, Chenzhou, 423000, China.

Keywords: Tobacco, Leaf nitrogen content, Hyperspectral, Remote sensing, Multivariate linear model

Abstract

In order to accurately and effectively obtain the nitrogen content of tobacco leaves during the whole growth period, in the present study the field canopy spectrum of the three critical periods of tobacco rosette stage, vigorous growth stage and topping stage were used. The correlation analysis of field canopy spectrum, first derivative spectrum, hyperspectral parameters and vegetation index with the nitrogen content of tobacco leaves was carried out one by one, and the prediction model was established by multiple linear regression using the variables with the best correlation coefficient. Results showed that the first derivative spectrum, EVI II and green peak position had strong correlation, which is suitable for introducing multivariate equations as independent variables. Finally, the modeling determination coefficient (R^2) was 0.66, RMSE was 0.40, and MAPE was 11%. The validation results showed that R^2 was 0.73, RMSE was 0.38, and MAPE was 8.33%, which proved that this model could accurately predict the nitrogen content of tobacco leaves and could meet the requirements of large-scale statistical monitoring of tobacco quality indicators in the field.

Introduction

Tobacco (*Nicotiana tabacum* L.) is one of the main cash crops in China. Continued efforts have been made to improve the tobacco yields along with rising living standards. Nevertheless, higher requirements still need to be met when it comes to tobacco quality, and better tobacco quality can bring greater economic benefits. The nitrogen content of tobacco leaves is one of the important indicators to reflect the growth status of tobacco in the field.

Alinat *et al.* (2015) reported that the nitrogen content of tobacco leaves has a direct bearing on the gene expressions of nitrogen metabolism-related enzymes and on the amount of nitrogen metabolites. Such an impact usually persists throughout the entire growth period of tobaccos, thereby affecting tobacco leaf quality. For example, Su *et al.* (2021) studied tobacco cultivar and analyzed the optimal fertilization amounts of nitrogen (N)-phosphorus (P)-potassium (K) fertilizers. They found that an ideal NPK fertilizer ratio promoted tobacco growth, and its influence on tobacco quality was by no means negligible. Hyperspectral remote sensing, originating in the 1920s, offers an important tool for experimental science, and this technique can be used to identify molecular and atomic structures (Fan *et al.* 2022). Since different biochemical components of crops have distinct absorption bands (El-Naggar *et al.* 2021), it is feasible to monitor crop quality parameters based on optical remote sensing data. The use of hyperspectral imaging in tobaccos has been more intensively studied in the following aspect: Prediction models for leaf area index, biomass, and quality indicators of tobacco are preliminarily established based on the original spectral reflectance, differential transformation, vegetation indice, area variable, and position variable obtained by hyperspectral imaging as independent variables. Such prediction

*Author for correspondence: <349632597@qq.com>. [1]Hunan Tobacco Company Chenzhou Company, Chenzhou, 423000, China.[2]Hunan Tobacco Company, Changsha, 410007, China.[3]Hunan Tobacco Company Changsha Company, Changsha, 410000, China.

models can be used to estimate and monitor tobacco growth and tobacco leaf quality (Cai *et al.* 2017). Svotwa *et al.* (2013) estimated tobacco yield at high precision and efficiency using a drone. They further built a yield estimation model based on multispectral data ($R^2 > 0.7$), which provided a theoretical basis for small-scale tobacco yield estimation. Gu *et al.* (2016) extracted the flue-cured tobacco growing area by combining the multispectral data with the object-oriented method, achieving an accuracy of 90.95%.

Multispectral imagery is one of the key sources of remote sensing data for tobacco monitoring, especially for tobacco yield estimation (Wang *et al.* 2015, Guo *et al.* 2019, Huang *et al.* 2021, Divyanth *et al.* 2022). In fact, hyperspectral images contain more continuous and a larger number of wavebands than multispectral images. The former can more precisely differentiate between surface features, facilitating the analysis of surface features based on spectral characteristics (Chen *et al.* 2021, Xu and Cui 2021,). The requirements on tobacco quality are no less strict than those on tobacco yield. In the present study, the quantitative relationship between the nitrogen content of tobacco leaves and hyperspectral variables in three developmental stages, namely, rosette stage, vigorous growth stage, and topping stage were analyzed. Besides, the hyperspectral prediction model for nitrogen content of tobacco leaves was established. The changes in the model's hyperspectral prediction ability for nitrogen content of tobacco leaves were characterized across the developmental stages. The influence of multi-stage combination on the performance of the prediction model was also discussed.

Materials and Methods

The study area was located in the tobacco experimental base in Guiyang County, Chenzhou City of Hunan Province. Continuous experiments for two consecutive years (2021 and 2022) were conducted using a randomized block design and involving three tobacco cultivars, namely, Xiangyan 5, Xiangyan 7, and Yunyan 87. These three cultivars were grown in three independent test plots, with five different N fertilizer treatments in each. N0: No fertilization, N1: Local fertilization amount*0.5, N2: Local fertilization amount, N3: Local fertilization amount*1.5, N4: Local fertilization amount*2. These treatments corresponded to severe nitrogen deficiency, mild nitrogen deficiency, appropriate amount of nitrogen fertilization, excessive nitrogen fertilization, and severely excessive nitrogen fertilization, respectively. Three replicates were set up for each treatment, and a total of 45 plots were involved in the experiments. Each plot measured 3.6 × 7.5 m, and the area between two adjacent plants was 1.2 × 0.5 m.

Analytical Spectral Devices (ASD) Fieldspec 3 Hi-Res spectroradiometer (350-2500 nm) was used for the measurement, with a sampling interval of 1.3 mm (for 350-1000 nm) and 2 nm (for 1000-2500 nm). Spectra were collected at 10:30-14:00 Beijing Time on a sunny day without wind or with very low wind speed. The full field of view of the spectroradiometer was 25°C, with the probe measuring vertically downwards at 0.6 m from the canopy top. The measurements were repeated 10 times within the field of view, and the average was taken as the reflectance spectrum at this particular point. Before and after measurements for each treatment, correction was performed using the reference board (the site for each measurement was randomly chosen within the plot). Spectral measurement was performed once at 40, 50 and 60 days after transplanting, respectively. Tobacco samples were collected after the spectral measurement in a synchronous or quasi-synchronous manner, followed by laboratory parameter determination.

The tobacco leaves samples collected at three different stages were further classified based on the potassium fertilization treatment. The total nitrogen content of each tobacco leaf was determined by semi-micro-sample distillation. Thus, the measured nitrogen contents of tobacco leaf samples in each plot were obtained.

It was found through literature review that the red, yellow and blue edge spectral parameters have been frequently used in crop quality monitoring and forecast (Curran 1989, Lamb *et al.* 2002, Olivares Díaz *et al.* 2019, Zhu *et al.* 2022). In the present study, the following spectral parameters were screened and chosen useful ones to build the prediction model: field canopy spectra, first-order derivative spectra of the field canopy, five vegetation indices (NDVI, RVI, EVI, DVI, and TVI), three-edge parameters (red, blue, and yellow edges), red valley position, and green peak position (Table 1).

Table 1. Selected vegetation indices and hyperspectral bands.

Type		Symbol	Name	Definition	
Derivative		ρ_i'	First derivative	$(R_i+1-R_i-1)/(x_i+1-x_i-1)$	(Gong *et al.* 2002)
Vegetation index		NDVI	Normalized difference vegetation index	(NIR-R)/(NIR+R)	(Huete, A. R. 1988)
		DVI	Difference vegetation index	NIR-R	(Gitelson *et al.* 2002)
		RVI	Ratio vegetation index	R/NIR	(Pearson and Miller 1972)
		EVI	Enhanced vegetation index	2.5(NIR-R)/(1+NIR+6R-7.5B)	(Jiang *et al.* 2008)
		TVI	Conversion vegetation index	$\sqrt{NDVI + 0.5}$	(Qian *et al.* 2022)
Hyperspectral characteristic parameters	Green mountain	R_g	Green peak reflectivity	Maximum spectral reflectance in the green light range	(Gong *et al.* 2002)
		λ_g	Green edge	*Rg* corresponds to the wave-length position	(Gong *et al.* 2002)
	Red valley	R_o	Red Valley Reflectivity	Minimum spectral reflectance in the red-light range	(Gong *et al.* 2002)
		λ_o	Red Valley Location	Wavelength position corresponding to *Ro*	(Gong *et al.* 2002)
		λ_r	Red edge position	Wavelength position corresponding to *Dr*	(Gong *et al.* 2002)
	Red edge	D_r	Red edge amplitude	Maximum value of first derivative spectrum in red edge	(Gong *et al.* 2002)
		SD_r	Red edge area	Area of first derivative spectrum in red edge	(Gong *et al.* 2002)
		λ_b	Blue edge position	Wavelength position corresponding to *Db*	(Gong *et al.* 2002)
	Blue edge	D_b	Blue edge amplitude	Maximum value of first derivative spectrum in blue edge	(Gong *et al.* 2002)
		SD_b	Blue edge area	Area of the first derivative spectrum in the blue edge	(Gong *et al.* 2002)
		λ_y	Yellow edge position	Wavelength position corresponding to *Dy*	(Gong *et al.* 2002)
	Yellow edge	D_y	Yellow edge amplitude	Maximum value of first derivative spectrum in yellow edge	(Gong *et al.* 2002)
		SD_y	Yellow edge area	Area of first derivative spectrum in yellow edge	(Gong *et al.* 2002)

Ri is the value of spectral reflectance at i in the range of 350 ~ 2500 nm. NIR is any spectral reflectance in the range of 780-2500 nm. Red is any spectral reflectance in the range of 620 ~ 700nm.

Spectral data were collected for two consecutive years (2021 and 2022) during the experiments. The total sample size was 180. Ninety samples collected in the first year constituted the training set, and those in the second year the validation set.

A multiple linear regression model consisting of several parameters was built and represented by the following equation:

$$y=b_0+b_1x_1+b_2x_2+b_nx_n+e \qquad (1)$$

where y is the dependent variable; *x1, x2, …, xn* are *n* independent variables involved in the modeling; *b0, b1, b2, and bn* are the corresponding constant terms of these independent variables, respectively. *e* is the error term.

The following performance indicators of the model were chosen: R^2 (coefficient of determination), root mean square error (RMSE), and mean absolute percentage error (MAPE).

$$R^2 = \frac{\sum_{i=1}^{n}(x_i-\hat{x}_i)^2}{\sum_{i=1}^{n}(x_i-\bar{x})^2} \qquad (2)$$

$$\mathrm{RMSE} = \sqrt{\frac{\sum_{i=1}^{n}(x_i-\hat{x}_i)^2}{n}} \qquad (3)$$

$$\mathrm{MAPE} = \frac{\sum_{i=1}^{n}\left|\frac{x_i-\hat{x}_i}{\hat{x}_i}\right|}{n} \times 100\% \qquad (4)$$

where *n* is the number of sample sets; $\bar{x}$ is the measured nitrogen content of the tobacco leaf; *xi* is the measured value of nitrogen content in tobacco leaf; $\hat{x}i$ is the predicted value of the model.

The higher the value of R^2, the higher the fitting degree of the model would be. RMSE and MAPE are accuracy measures of predictions from the regression model. The smaller the RMSE and MAPE, the more accurate the predictions.

Results and Discussion

Canopy spectra were determined at three key developmental stages, namely, rosette stage, vigorous growth stage, and topping stage. For the sake of practicality and validity, invalid wavebands with abnormal fluctuations beyond 150 nm were deleted. The remaining frequency range from 350 to 1500 nm was used for correlation analysis and for finding the first-order derivatives. The results are shown in Figs 1 and 2.

As analyzed from Fig. 1, within the visible frequency range of 350 to 750 nm, the coefficient of correlation between the spectral reflectance and nitrogen content of tobacco leaves increased, peaking at about 693 nm. Within the infrared frequency range of 800 to 1350 nm, the coefficient of correlation between the spectral reflectance and nitrogen content of tobacco leaves seemed to stabilize. However, the coefficient of correlation fluctuated abnormally in the frequency range of 1350 to 1500 nm. This finding might be attributed to water absorption and instrument sensitivity.

The first-order derivative of the original spectral reflectance and performed a correlation analysis against the nitrogen content of tobacco leaves were calculated. The calculation result was compared against the coefficient of correlation between the original spectral reflectance and nitrogen content of the tobacco leaves. Sensitive wavebands were identified (those with a coefficient of correlation above 0.4 were considered sensitive), and the distribution pattern was analyzed. As analyzed from Fig. 2, sensitive wavebands in the original spectra were mainly concentrated within the visible frequency range of 500 to 800 nm. On the first-order derivative spectra, apart from the sensitive wavebands in the visible frequency range of 350 to 700 nm, the number of such wavebands also increased dramatically within the infrared frequency range of 900 to 1500 nm.

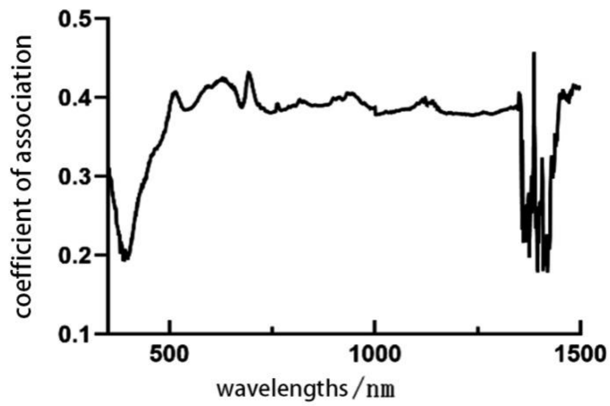

Fig. 1. Correlation analysis of canopy spectra in whole growth period.

As shown in Fig. 2 and Table 2, the range of sensitive wavebands was greatly expanded after finding the first-order derivative of the original reflectance. Besides, the degree of correlation also increased on the first-order derivative spectra. On the original spectra, the maximum coefficient of correlation in the sensitive wavebands ranged between 0.40 and 0.43. The maximum coefficient of correlation increased to 0.69 on the first-order derivative spectra.

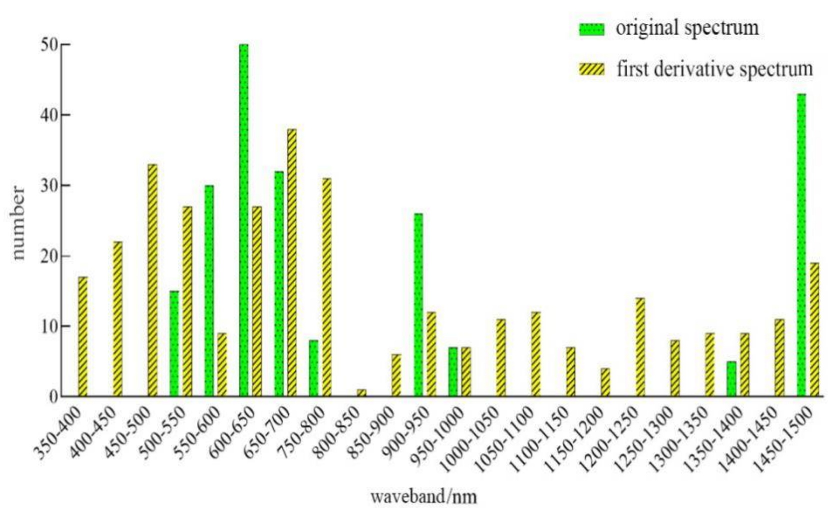

Fig. 2. Distribution of sensitive band of original spectrum and first derivative spectrum in whole growth period.

Table 2. The best sensitive band of the first derivative spectrum and the original spectrum in the whole growth period.

The original spectrum		First derivative spectrum	
Optimum sensitive band	r	Optimum sensitive band	r
693nm	0.43	1095nm	0.609

In the infrared and near-infrared frequency ranges, six spectral indices were calculated, namely, NDVI, RVI, DVI, TVI, EVI, and EVI II. A correlation analysis was performed between the measured value of the nitrogen content of tobacco leaves and each of the above spectral indices. Results presented in Table 3 showed that the coefficient of correlation between EVI II and the nitrogen content of tobacco leaves was the highest. Therefore, EVI II was introduced as an independent variable into the multiple linear regression model.

Table 3. Correlation analysis between leaf nitrogen content and vegetation index of tobacco in whole growth period.

	NDVI	RVI	DVI	TVI	EVI	EVIII
Growth duration	Correlation coefficient	Correlation coefficient	Correlation coefficient	Correlation coefficient	Correlation coefficient	Correlation coefficient
	-0.253	0.251	-0.351	-0.252	-0.406	**-0.453**

Such spectral characteristic parameters as red valley position, green peak position, and three-edge parameters were calculated and then subjected to normalization and differential calculation. A correlation analysis was performed between each of these parameters and nitrogen content of tobacco leaves using the SPSS software. Results are shown in Table 4.

Table 4. Correlation analysis of spectral characteristic parameters in whole growth period.

Characteristic parameter	Pearson correlation coefficient	Characteristic parameter	Pearson correlation coefficient
R_g	-0.207	SD_b	**-0.376****
R_o	-0.209	R_g/R_o	-0.023
λ_g	**-0.458****	*SDr-SDy*	-0.051
λ_o	0.142	*SDr-SDb*	0.139
λ_r	**0.404****	*SDb-Sdy*	**-0.342****
λ_y	0.047	*SDr/SDb*	**0.355****
λ_b	0.278*	*SDr/SDy*	-0.277
D_r	-0.201	*SDb/SDy*	**0.345****
D_b	**-0.357****	*(Rg-Ro)/(Rg+Ro)*	-0.060
D_y	-0.008	*(SDr-SDy)/(SDr+SDy)*	**-0.324****
SD_r	-0.051	*(SDr-SDb)/(SDr+SDb)*	**0.391****
SD_y	0.270*		

R_g and R_o are green peak and red valley, λ_g, λ_o, λ_r, λ_y and λ_b are green peak, red valley, red edge, yellow edge and blue edge respectively, *Dr*, *Db* and *Dy* are red edge, blue edge and yellow edge respectively, SD_r, SD_y and SD_b are red edge, blue edge and yellow edge respectively.

A prediction model was established using multiple linear regression. Specifically, a prediction model was built using the combination of two or three independent variables, respectively. The optimal combination of parameters was determined on this basis. The models built using three different combinations of independent variables were compared, as shown in Table 5. It was found that the R^2 of the model based on the combination of vegetation index, reflectance and spectral parameter was higher than that of the other two models. This prediction model was represented by $Y = 386.6 + 0.76*\rho1095' - 1.46* EVIII - 0.69*\lambda g$.

Table 5. Multiple linear regression prediction model for tobacco nitrogen content.

Parameter combination	Prediction model of tobacco leaf content	R^2
Reflectance plus spectral parameters	$Y = 354.3-0.63*\lambda_g +0.14* \rho_{1095}'$	0.55
Reflectance plus vegetation index	$Y = 3.038-1.33* \rho_{1095}' +2.15* EVIII$	0.49
Vegetation index plus reflectance plus spectral parameters	$Y = 386.6+0.76*p_{1095}' -1.46* EVIII-0.69*\lambda_g$	0.66

p_x' is the first derivative of the original spectral reflectance at *xnm*, λ_g is the green peak position, Y is the nitrogen content of tobacco leaves.

The above three multiple linear regression models were assessed and validated. The validation dataset was a fully independent dataset. The validation results presented in Table 6 showed that $R^2 = 0.66$ for the multiple linear regression model based on the combination of the three independent variables, and $R^2 = 0.73$ for the validation. Both were higher than those of the model based on the combination of two independent variables. Thus, the model based on the combination of three independent variables, namely, EVI II, first-order spectral reflectance, and green peak position, was the optimal model for predicting the nitrogen content of tobacco leaves throughout the entire growth period. The RMSE of this model was 0.15, and MAPE was 8.33%. The model assessment is shown in Fig. 3.

Table 6. Comparison of multiple linear regression models.

Model	R^2	RMSE	MAPE
$Y = 354.3-0.63*\lambda_g +0.14* \rho_{1095}'$	0.66	2.99	30%
$Y = 3.038-1.33* \rho_{1095}' +2.15* EVIII$	0.53	0.44	13%
$Y = 386.6+0.76* \rho_{1095}' -1.46* EVIII-0.69*\lambda_g$	0.73	0.38	8.33%

The present study focused on the monitoring of nitrogen content in tobacco leaves based on multiple linear regression modeling. The linear model was easy to construct and involved simple calculation. But given the multicollinearity among vegetation indices and hyperspectral parameters, it was not possible to introduce several strongly correlated vegetation indices or spectral parameters simultaneously into the multiple linear regression model. The present method had certain defects due to this fact. In the future, some research on nitrogen content prediction in tobacco leaves based on partial least-squares regression (PLS) and principal component analysis (PCA), which can overcome the intrinsic defects in linear models and increase the monitoring accuracy may taken up. The sensitive bands selected by the models established by these two algorithms are basically concentrated in the range of 780 - 1800nm (Wu and Shi 2004, Xie *et al.* 2014, Sampaio *et al.* 2018, Peiris *et al.* 2020, Zhao *et al.* 2022), which provides reference for a deeper investigation.

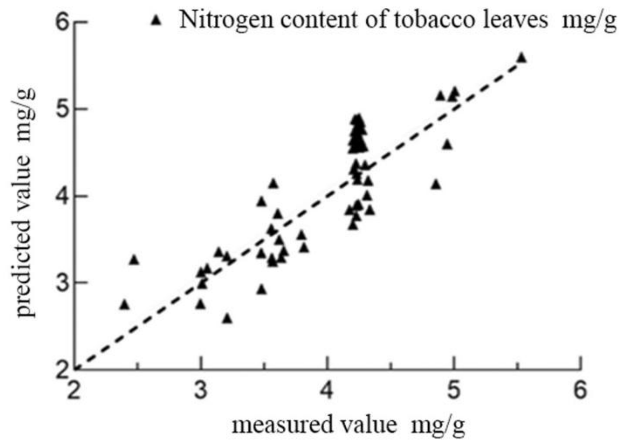

Fig. 3. Multivariate linear regression model evaluation.

As for the sensitive wavebands for nitrogen detection, many scholars believe that the near-infrared frequency range is more sensitive to nitrogen content. For example, Moharana and Dutta (2016) found that the frequency range sensitive for nitrogen content of rice was 760 to 900 nm. Fu *et al.* (2021) showed that the spectral index NDVI could be suitably used for an accurate prediction of nitrogen content of wheat leaves. Others have built a high-accuracy prediction model for nitrogen content in rice within the visible frequency range. For example, Yang *et al.* (2020) built the prediction model using the first-order differential spectrum at 751 nm and rice leaf nitrogen concentration, with the coefficient of correlation reaching 0.841.

At present, studies on tobacco quality are still facing some difficulties. In the future, satellite data may be combined with data from multiple platforms, including drones, for relevant investigations. The recent emergence of big data tools makes the development of new algorithms possible, so as to dramatically improve the monitoring accuracy.

The present study was concerned with nitrogen content estimation of tobacco leaves throughout the entire growth period. The main influence factors of nitrogen content in tobacco leaves were analyzed under five different potassium fertilization treatments. A multiple linear regression model was built based on the combination of the vegetation index, first-order derivative spectral reflectance, and spectral characteristic parameter. Results showed that the potassium fertilization amount had no direct impact on the nitrogen content of tobacco leaves. The coefficient of determination was 0.66 for the model thus built, the RMSE being 0.40 and MAPE 11%. The correlation of determination during the validation experiment was 0.73, RMSE was 0.38, and MAPE was 8.33%.

It was found that the first-order derivative of canopy spectra resulted in an expansion of wavebands sensitive to nitrogen content. The prediction model based on a combination of parameters increased the prediction accuracy for nitrogen content of tobacco leaves. However, this observation needs to be verified in other tobacco cultivars grown in different regions, so as to improve the accuracy and applicability of the prediction model.

Acknowledgements

This work was partly financially supported in part by the Hunan Tobacco Company Chenzhou Company Science and Technology Project (CZYC2021JS08).

References

Alinat E, Delaunay N, Archer X, Mallet JM and Gareil P 2015. A new method for the determination of the nitrogen content of nitrocellulose based on the molar ratio of nitrite-to-nitrate ions released after alkaline hydrolysis. J. Hazardous Mat. **286**: 92-99.

Cai H, Di X and Jin G 2017. Allometric models for leaf area and leaf mass predictions across different growing seasons of elm tree (Ulmus japonica). J. Forestry Res. **28**(5): 975-982.

Chen XJ, Pan W, Tian QL and Zhang C 2021. Application of hyperspectral images in digital record of drill cores. Paper presented at the Proc. SPIE. **11763**: id. 1176352 6 pp. (2021).

Curran PJ 1989. Remote sensing of foliar chemistry. Remote Sensing Environ. **30**(3): 271-278.

Divyanth LG, Chakraborty S, Li B, Weindorf DC, Deb P and Gem CJ 2022. Non-destructive prediction of nicotine content in tobacco using hyperspectral image–derived spectra and machine learning. J. Biosyst. Engin. **47**(2): 106-117.

El-Naggar AG, Jolly B, Hedley CB, Horne D, Roudier P and Clothier BE 2021. The use of terrestrial LiDAR to monitor crop growth and account for within-field variability of crop coefficients and water use. Comput. Electron. Agricul. **190**: 106416.

Fan Z, Wang D, Zhang N and Zhou B 2022. Monitoring of nitrogen transport in pear trees based on ground hyperspectral remote sensing and digital image information. J. Chem. **2022**: 7590846.

Fu Z, Yu S, Zhang J, Xi H, Gao Y, Lu R, Zheng H, Zhu Y, Cao W and Liu X. 2021. Combining UAV multispectral imagery and ecological factors to estimate leaf nitrogen and grain protein content of wheat. Europ. J. Agron. **132**: 126405.

Gitelson AA, Kaufman YJ, Stark R and Rundquist D 2002. Novel algorithms for remote estimation of vegetation fraction. Remote Sensing Environ. **80**(1): 76-87.

Gong P, Pu R and Heald RC 2002. Analysis of in situ hyperspectral data for nutrient estimation of giant sequoia. Intern. J. Remote Sensing **23**(9): 1827-1850.

Gu L, Xue L, Song Q, Wang F, He H and Zhang Z 2016. Classification of the fragrant styles and evaluation of the aromatic quality of flue-cured tobacco leaves by machine-learning methods. J. Bioinfor. Comput. Biol. **14**(06): 1650033.

Guo T, Tan C, Li Q, Cui G and Li H 2019. Estimating leaf chlorophyll content in tobacco based on various canopy hyperspectral parameters. J. Ambient Intell. Humanized Comput. **10**(8): 3239-3247.

Huang L, Wu X, Peng Q, and Yu X 2021. Depth Semantic segmentation of tobacco planting areas from unmanned aerial vehicle remote sensing images in plateau mountains. J. Spectroscopy **2021**: 6687799.

Huete AR 1988. A soil-adjusted vegetation index (SAVI). Remote Sensing Environ. **25**(3): 295-309.

Jiang Z, Huete AR, Didan K and Miura T 2008. Development of a two-band enhanced vegetation index without a blue band. Remote Sensing Environ. **112**(10): 3833-3845.

Lamb DW, Steyn-Ross M, Schaare P, Hanna MM, Silvester W and Steyn-Ross A 2002. Estimating leaf nitrogen concentration in ryegrass (*Lolium* spp.) pasture using the chlorophyll red-edge: Theoretical modelling and experimental observations. International J. Remote Sensing **23**(18): 3619-3648.

Moharana S and Dutta S 2016. Spatial variability of chlorophyll and nitrogen content of rice from hyperspectral imagery. ISPRS J. Photogram. Remote Sensing, **122**: 17-29.

Olivares Díaz E, Kawamura S, Matsuo M, Kato M and Koseki S 2019. Combined analysis of near-infrared spectra, colour, and physicochemical information of brown rice to develop accurate calibration models for determining amylose content. Food Chemistry **286**: 297-306.

Pearson R and Miller L 1972. Remote Mapping of Standing Crop Biomass for Estimation of Productivity of the Shortgrass Prairie. Proceeding of the 8th International Symposium on Remote Sensing of Environment -1: 1355.

Peiris KHS, Bean SR, Tilley M and Jagadish SVK 2020. Analysis of sorghum content in corn–sorghum flour bioethanol feedstock by near infrared spectroscopy. J. Near Infrared Spectr. **28**(5-6): 267-274.

Qian B, Ye H, Huang W, Xie Q, Pan Y, Xing N 2022. A sentinel-2-based triangular vegetation index for chlorophyll content estimation. Agricul. Forest Meteorol. **322**: 109000.

Sampaio PS, Soares A, Castanho A, Almeida AS, Oliveira J and Brites C 2018. Optimization of rice amylose determination by NIR-spectroscopy using PLS chemometrics algorithms. Food Chem. **242**: 196-204.

Su J, Chen Y, Zhu Y, Xiang J, Chen Y and Hu B 2021. The response of Hongda, a flue-cured tobacco cultivar, to nitrogen fertilizer rate. Arch. Agron. Soil Sci. **67**(4): 536-550.

Svotwa E, Masuka AJ, Maasdorp B, Murwira A and Shamudzarira M 2013. Remote sensing applications in tobacco yield estimation and the recommended research in Zimbabwe. ISRN Agron. **2013**: 941873.

Wang K, Zhou ZF, Liao J and Fu Y 2015. The application of high-resolution SAR in mountain area of karst tobacco leaf area index estimation model. J. Coastal Res. **73**(sp1): 415-419.

Wu JG and Shi CH 2004. Prediction of grain weight, brown rice weight and amylose content in single rice grains using near-infrared reflectance spectroscopy. Field Crops Res. **87**(1): 13-21.

Xie LH, Tang SQ, Chen N, Luo J, Jiao GA and Shao GN 2014. Optimisation of near-infrared reflectance model in measuring protein and amylose content of rice flour. Food Chem. **142**: 92-100.

Xu Y and Cui G 2021. Influence of spectral characteristics of the Earth's surface radiation on the greenhouse effect: Principles and mechanisms. Atmospheric Environ. **244**: 117908.

Yang J, Du L, Cheng Y, Shi S, Xiang C and Sun J 2020. Assessing different regression algorithms for paddy rice leaf nitrogen concentration estimations from the first-derivative fluorescence spectrum. Opt. Express **28**(13): 18728-18741.

Zhao W, Wu J, Shen Q, Liu L, Lin J and Yang J 2022. Estimation of the net primary productivity of winter wheat based on the near-infrared radiance of vegetation. Sci. Total Environ. **838**: 156090.

Zhu C, Ding J, Zhang Z, Wang J, Wang Z and Chen X 2022. SPAD monitoring of saline vegetation based on Gaussian mixture model and UAV hyperspectral image feature classification. Comput. Electron. Agricul. **200**: 107236.

(Manuscript received on 28 March, 2023; revised on 12 July, 2023)